



Micromachining using the high energy flat-top beam of a femtosecond pulse UV laser system: micropillar prefabrication

Péter Imre Szabó^{1,2} · Dávid Ugi³ · Barnabás Gilicze¹ · Zoltán Dankházi³ · Sándor Lipcsei³ · Zsolt Homik¹ · Zsolt Tóth^{1,4}

Received: 8 December 2022 / Accepted: 25 April 2023 / Published online: 9 May 2023
© The Author(s) 2023

Abstract

Ablation with ultrashort laser pulses as a surface micromachining tool was studied using a hybrid die-excimer laser system that has high energy per laser pulse (tens of mJ's), about 600 fs pulse duration and low repetition rate (2 Hz). The effect of ablation on the material microstructure with this high energy pulsed laser system was studied. Micropillars were fabricated by laser ablation using a spot size of hundreds of micrometers. Two methods were tested for micromachining. Multiple laser pulse ablation on a standing sample resulted in a columnar microstructure around the micropillars. This unwanted structure was avoided by beam scanning, resulting in a rather homogeneous ditch. By HR-EBSD measurement it was found that the heat affected zone is less than 1 μm , which was confirmed by numerical temperature simulations, too. The dislocation density measured below the specimen surface was unaltered, meaning that no significant crystal degradation occurred. In summary, large-scale micro objects with a diameter in the order of 100 μm without significant change in the crystalline microstructure below the surface, like large-scale micropillars for compression tests, can be fabricated.

Keywords Femtosecond laser ablation · Micromachining · Microstructure · Dislocation density · Micropillar fabrication

1 Introduction

Surface machining can be performed using several techniques depending on the required accuracy or the required modification or preservation of the structure of the material. Laser systems have various applications, one of them is machining and micromachining. If the pulse energy of a laser system is high enough, it can be used for removal of

material, that is called laser ablation. Since laser systems can produce very stable and controllable pulses, they can be an appropriate tool for precise surface micromachining [1–3]. In some cases the machined object needs to meet very strict characteristics. One of these cases is the fabrication of micropillars for deformation tests.

Plastic deformation of microscale specimens like microscale columnar objects, i.e., micropillars, has been an emerging research area of metals and other materials in the last two decades [4–14]. These deformation tests show that plastic deformation of objects with size of a few microns is significantly different from the deformation of macro-sized objects. Their deformation curves show a very complex and individual behavior, and is strikingly different for each and every specimen. This particular behavior is unpredictable and is very sensitively dependent on almost all aspects of the experimental conditions, e.g. microstructure, dislocation configuration and deformation mode [15–18]. It means that to measure the true statistics of the plastic deformation of the given sample, the fabrication process must not modify the original microstructure of the volume where the deformation will take place during the compression test. Thus the measured deformation curve is determined only by the

✉ Péter Imre Szabó
szabo.peter.imre@uni-nke.hu; pszabo@metal.elte.hu
Zoltán Dankházi
zoltan.dankhazi@ttk.elte.hu
Zsolt Tóth
ztoth@physx.u-szeged.hu

¹ High Intensity Laser Laboratory (HILL), Institute of Physics, University of Szeged, Dóm tér 9, Szeged 6720, Hungary
² Department of Natural Science, University of Public Service, Budapest 1441, Hungary
³ Department of Materials Physics, Eötvös Loránd University, Pázmány Péter sétány 1/A, Budapest 1117, Hungary
⁴ Department of Medical Physics and Informatics, University of Szeged, Korányi fasor 9, Szeged 6720, Hungary

original material properties. Often for these tests microscale columnar objects, micropillars are fabricated and compressed. These objects are machined into a bulk specimen, often single crystal, by focused ion beam (FIB) milling. The FIB technology is suitable for very exact micromachining, for example this is a common and widespread technology for manufacturing ~ 50 nm thin samples for transmission electron microscopy [19]. Or, for the fabrication of micropillars, a vertical ditch can be milled around a circle or a square on the specimen surface, resulting in a column with a constant cross section, creating a straight column. During FIB milling the left over material, which is the pillar, is not altered in the characteristics that determine plastic deformation. Some ions get implanted close to its surface [20], but the dislocation structure is not altered [21].

FIB manufacturing is a precise tool for nano- or micro-manufacturing, but is ineffective for fabrication of larger pillars [22] due to the low material removal time-rate. Thus by FIB only fabrication of objects of dimensions of maximum few tens of microns is possible. Therefore producing objects, in our case, pillars, which would bridge the micro- and macroscale, are almost impossible. Recently, as a new approach, femtosecond laser ablation has been introduced to produce larger micropillars [23–29], tensile test dog-bones [30] or cantilevers [31]. Its high material removal rate and its low effect on the material microstructure mean that it can be a tool to produce or prefabricate larger pillars, or any larger microscale object. Prefabrication, that needs to be finalized by FIB milling, is doubly useful. On the one hand, by prefabrication much of the material is removed. On the other hand the FIB milling of a prefabricated pillar is much faster since the material removal rate of the FIB milling also depends on the angle between the ion beam and the surface normal [32]. This means that straightening and polishing an existing wall is preferable to trenching. Therefore, prefabrication improves the finalization FIB processing significantly.

The advantage of ultrashort pulses compared to longer pulses is that while they can provide a significant material removal rate, ultrashort laser pulses cause low degradation in the material surrounding the ablated spot, heat transfer from the irradiated spot is negligible. The heat affected zone (HAZ) that surrounds the ablated spot is very thin [26, 33], and recently it has been found that lattice defects like dislocations that would modify the plastic deformation properties of the specimen, are not injected far from the area of laser ablation [28, 34, 35]. Thus it can be suitable for micropillar fabrication.

The goal of this work is to investigate the effects of laser ablation on the left over material (the produced pillar) using a high energy per pulse UV laser system. These effects can stem from various phenomena, e.g. recrystallization due to heat transport, effect of mechanical shocks caused by the expansion of the material being ablated (dislocation creation

and injection, fatigue) or the related light-material interaction (method of excitation, photon energy) and many others.

2 Experimental setup

The hybrid dye-KrF excimer laser system used is described in detail elsewhere [36, 37], here we summarize only the properties that are important for the micromachining and give a short description of the pulse generation. It provides ultrashort, 600 fs long pulses at the wavelength of 248.5 nm. The output beam has a square-shape cross section with side length of 4 cm. The beam profile has a super-Gaussian energy distribution, which can be characterized by a flat top distribution in the center of the beam. The pulses are generated by several, consecutive steps in the laser system. Firstly a seed pulse is generated by a distributed feedback dye laser. After consecutive steps of amplifying through other dye lasers and beam shaping the pulse serves as a seed of an amplifier of 497 nm wavelength and Gaussian-distribution. This, after frequency doubling, serves as a seed pulse of the final, KrF excimer amplifier, giving an UV pulse. Its Kr and F medium is excited by an electric discharge, creating a KrF excited dimer medium. The pulse passes through this medium, thus is amplified, four times. Regarding the spatial distribution of the laser beam, the output has a flat-top like distribution, because the cross section of the discharge inside the KrF excimer amplifier has a square-like distribution. There are several processes which influence the spatial distribution of the beam. The frequency conversion before the UV amplification acts as a highly effective spatial filter. The amplification passes in the KrF medium affect the spatial distribution by the large gain, which leads to top hat profile. Spatial filtering is introduced before the final amplification stage to reduce the amplified spontaneous emission (ASE) and has a smoothing effect on the spatial distribution (reducing the role of the high spatial frequency components). In our experiments an aperture was used to transmit the most homogeneous part of the beam, where the energy density variation was less than 5%.

Using an aperture the most homogeneous part of the beam, where the energy density variation was less than 5%, was let through. The beam was masked then focused by a 46 cm focal length lens, thus achieving an energy density giving a high ablation rate. Firstly the beam was masked by an annular aperture and irradiated a standing sample. Secondly a square mask with side length of 2.5 cm was used with a moving sample. In the latter the sample was moved with a speed of $100 \mu\text{m/s}$ along linear segments. This was carried out on a custom-made moving stage, equipped with stepper motors controlled by a custom-made code through an Arduino controller. One step size was $2.5 \mu\text{m}$. The scanning velocity was chosen so that between two laser pulses

the laser spot was moved only by a fraction of its side length. The incident spot size was hundreds of μm 's. The pulse energy measured after the mask was 5 mJ and 20 mJ, respectively. Ablation was done in ambient air. To avoid plasma formation in the air, the sample surface was positioned within the focal distance, close to the focal point. For the sample processing 2 Hz repetition rate was used as it was the maximum repetition rate of the system.

In general, in the investigation of the dislocation dynamics pure single crystals are the most commonly used to avoid the effects caused by grain boundary and solute atom presence [4, 16]. Metals are also of common interest. Zinc is often used for micropillar compression tests as it gives a significant acoustic emission signal [38]. To select the sample, such features as availability, cost efficiency, and heat affect sensitivity, were considered. Since zinc has a low melting point and yield stress on certain lattice planes, single crystalline zinc was found to be the most suitable material.

Firstly polycrystalline zinc (Zn) samples were used for testing pillar fabrication by laser microfabrication. To test the effects of laser irradiation on the material microstructure a random oriented bulk zinc single crystal was machined. For its preparation first it was mechanically polished using AlOx particles with an average diameter of $1\ \mu\text{m}$. This was followed by electropolishing with Struers D2 electrolyte at 10 V and a maximum current of 2 A for 10 s. During this preparation process, the sample remains in a single crystal form verified by EBSD measurements. Microscopy was carried out to see the possible changes in the material microstructure induced by the laser ablation process. Firstly a Hitachi S-4700 field emission gun scanning electron microscope (FESEM) was used to capture low magnification, large depth of field electron images. For focused ion beam (FIB) polishing and high-resolution electron backscatter diffraction (HR-EBSD) investigations a FEI Quanta 3D dual-beam scanning electron microscope (SEM with field emission gun and FIB) was used.

3 Temperature calculations

The processes initiated by ultrashort pulse laser ablation are extremely complex: electron excitation, electron–electron and electron–lattice interactions [39, 40], phase transitions, material transport [41] can compete simultaneously during and after the laser pulse. Temperature profiles were calculated from the beginning of the laser pulse till 1 ns by a simple one-dimensional simulation, detailed in [42, 43]. The calculations were based on the numerical solution of the thermal diffusion equation using the method of finite differences. The starting temperature was 300K. The simulation took the reflection and absorption of the laser pulse into account, thus giving a more realistic result than an

estimation of the thermal diffusion length. For the calculations a custom made program was applied, written in Pascal code. The simulation took the temperature dependence of thermal properties into account. The thermal data of zinc, like the latent heat of melting, the latent heat of evaporation and specific heat was used to calculate the thickness of the layer, where the crystalline structure was disrupted and the material transformed to gaseous phase. The region that had a temperature above the vaporization temperature of zinc at atmospheric pressure (1180K) was considered to be ablated and removed. No heat exchange between this region and the region below this ablated layer was considered. Other effects like thermo-mechanical shocks, gas transport processes, plasma formation and plasma absorption (plasma shielding) were not included in the model.

With these simulations our goal is to compare our experimental results with the estimated temperature distributions.

4 Results and discussion

4.1 Laser ablation experiments

4.1.1 Standing target processing

The first experiments were performed using an annular aperture. The aim was to fabricate pillars with the aspect ratio as in [9, 44], which can be used for compression-deformation tests [4]. For these tests pillars with height of several μm 's are fabricated. For instance the pillars were $12\ \mu\text{m}$ high in [44]. Laser prefabrication of micropillars gives the possibility to fabricate larger pillars, for instance they were $50\ \mu\text{m}$ high in [24], but even higher pillars can be of interest. This amount of material to be removed has to be matched to the ablation rate, i.e., the thickness of the material removed per shots. The ablation rate is determined by the energy density of the focused laser beam [45–48]. Assuming a $150\ \mu\text{m}$ wide ditch around the pillar on both sides plus a pillar of the same width, the whole spot diameter for standing target processing needs to be $450\ \mu\text{m}$. Even with the high-energy (20 mJ per pulse) system used in our experiments the energy density is approximately $10\ \text{J}/\text{cm}^2$ in this case. Ablation of copper is measured in [46] and is also widely used for micropillar tests [24]. Based on the data of [46] an ablation rate of 200 nm/pulse can be approximated for $10\ \text{J}/\text{cm}^2$ fluence. From this it is easy to see that about 750 laser pulses are required to produce a column with a height of $150\ \mu\text{m}$.

However, it is known that femtosecond laser ablation of a single pulse creates a rough surface profile [49, 50], and ablation of several laser pulses creates a variety of surface structures with sizes ranging from hundreds of nanometers to several micrometers, even with the same height as the ablated ditch [51–53]. The applied ultrafast KrF laser has

higher coherence than ns excimer lasers, because it inherits the coherence of the seed pulse, which was generated by a distributed feedback dye laser. As a consequence, the scattering of the laser pulse from the irregularities or the edge of the mask may produce interference. LIPSS formation due to interference of the scattered and incoming laser light may initiate the cone structure formation as described in [54]. These columns could be an obstacle for the deforming pillar during the compression tests. Figure 1 shows a SEM image of a laser ablated area on a standing sample. The random columnar structure observed by others is present also after our micromachining process. This shows that it is not possible to create a free-standing microcolumn using a standing sample due to the columnar structure that is left over around it after laser ablation.

4.1.2 Scanning processing

An advanced beam homogenisation method has been developed for a similar laser system [55] that utilizes both two-photon absorption and variable beam displacement. In our second series of experiments a scanning method was applied to create a homogeneous ditch, to fabricate a free-standing pillar. The sample was moved along a line. Therefore we implemented beam displacement only. This method has the benefit of averaging the beam in the direction of scanning. To test this method two intersecting lines were ablated onto the specimen, shown in Fig. 2.

It shows that beam scanning is an effective way of homogenizing in the scanning direction: no large undulating columns can be observed, the ditch is homogeneously deep in this direction. However, ablation was not homogeneous in the direction perpendicular to the scanning direction. A wavy structure was observed, which was likely the

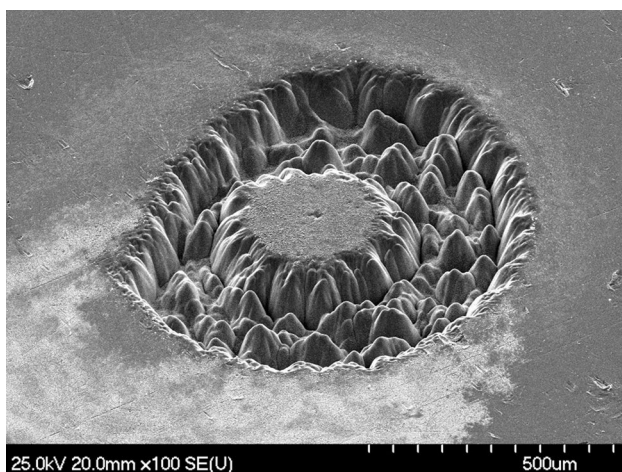


Fig. 1 SEM image of the sample surface that was ablated with a standing target

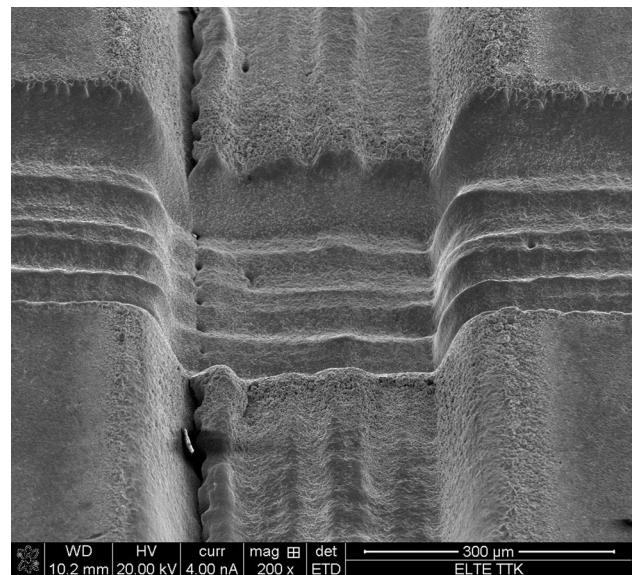


Fig. 2 Two intersecting straight lines ablated onto the sample using beam scanning in one direction. The columnar structure observed after static laser spot position is not present

consequence of diffraction and focusing. At the intersection of the two lines on Fig. 2 the superposition of the two wavy system can be observed.

This clearly demonstrates that the columnar structure that has approximately the same height as the ditch, shown on Fig. 1, was the effect of beam inhomogeneities in case of using this high-energy UV laser system with a zinc sample.

The beam scanning method was used to produce a pillar. The laser beam was scanned around the prospective pillar as illustrated in Fig. 3, resulting in an unablated region with the cross section of a square. During this the laser beam passed along linear segments that have a length of twice the spot size plus the pillar size.

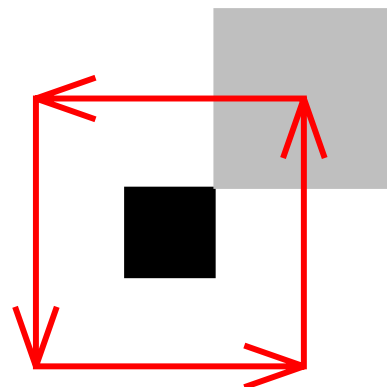


Fig. 3 Scanning path of the laser spot (grey) around the prospective pillar (black)

The scanning velocity was chosen so that between two laser pulses the laser spot was moved only by a fraction of its side length, the scanning speed was $100 \mu\text{m/s}$. The incident spot size was chosen to be hundreds of μm 's as it gave the best results.

The SEM image in Fig. 4 shows a pillar made using this method. Redeposition was observed both on the whole surface of the pillar and on the ditch and its vicinity. The brightness of the secondary electron image is increased by the redeposited oxide particles. The inner area of the SEM image, covered by the ablation products, can be well separated from the intact zinc surface, which has a darker shade in the outer regions. We tested placing the sample both horizontally and vertically, and a significant amount of redeposition was observed in both cases. After the laser ablation process, the redeposition must be removed to obtain a clean single crystal object.

4.2 Damage of the material microstructure and surface redeposition removal

The EBSD technology is able to reveal the crystal phase and orientation, and nowadays there is an emerging and widely accepted methodology for strain calculation from EBSD pattern shifts developed by Wilkinson et. al. [56]. The presence of lattice defects modify the distance between the lattice planes, therefore the electrons which are diffracted will travel to the detector on different paths, thus modifying the EBSD pattern. Using several steps of filtering, cross-correlation of the obtained Kikuchi-patterns and eventually

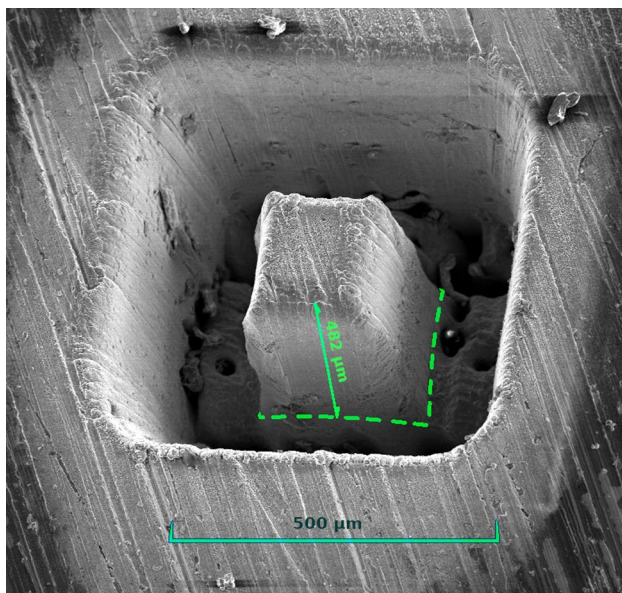


Fig. 4 A pillar fabricated with the described beam scanning method. The scale bar indicates the width of the pillar and the ditch, while the value on the picture indicates the height of the pillar

stress–strain calculations one may determine the so-called geometrically necessary dislocation (GND) density [57, 58]. The GND density corresponds to the density of the dislocations that are trapped due to strain gradient fields. It is a good measure to describe the geometrical arrangement of dislocation structures, the internal stress distribution of the system or the polarization state of the dislocation ensemble [59].

The laser ablation was carried out on a single crystal sample according to the section 4.1.2. The pillars were positioned onto the edge of the sample as it is required for EBSD measurements.

Figure 5a shows a pillar fabricated into a single crystal. It is covered by redeposited material. For high quality EBSD mapping this redeposited material on the pillar's surface must be removed. This was done by FIB polishing. Using FIB polishing an exact thickness of the surface can be removed, but only slowly, and on a small area. The FIB polishing was performed with a finishing Ga^+ current of 3 nA. The relatively low ion current and setting the ion beam parallel to the pillar's axis minimize the FIB effect on the crystalline structure and result in an EBSD ready surface. The pillar was FIB-polished close to its top as indicated in Fig. 5b, making possible the measurement of the crystal orientation and the GND density under the redeposited material. In our case, the deposits have porous structure, on the contrary to the original crystal, which makes them easily distinguishable, see Fig. 6a and b.

The measured GND density map and the crystal orientation map, obtained by the EBSD measurement, is presented in Fig. 6a and Fig. 6b, respectively. The calculated GND density values were the same as we measured previously on the same intact Zn single crystal, presented in the supplementary material of [38]. These results mean that the laser processing did not give any increment in the dislocation density, and the crystalline microstructure was preserved during the ablation process.

A thin layer is observed at the transition from the non-porous (crystalline) to the porous (redeposition) zone. This transition zone is indicated by the high GND density region (marked by deep purple colour) between the crystalline (orange colour) and the porous (white colour) parts in Fig. 6a. In this narrow layer higher dislocation density was measured not because of real dislocation content, but due to the sensitivity of the HR-EBSD technique. We assume that this layer is the heat affected zone. Its thickness is definitely smaller than $1 \mu\text{m}$. Note, that its real thickness is smaller than that is apparent in Fig. 6a, since the FIB cutting was performed with a low inclination angle, i.e. the angle between the pillar surface and the direction of the ion beam, that resulted in an oblique cutting in depth. This is in a good agreement with the results of [26, 28, 33–35], but it is important to emphasize the difference between the

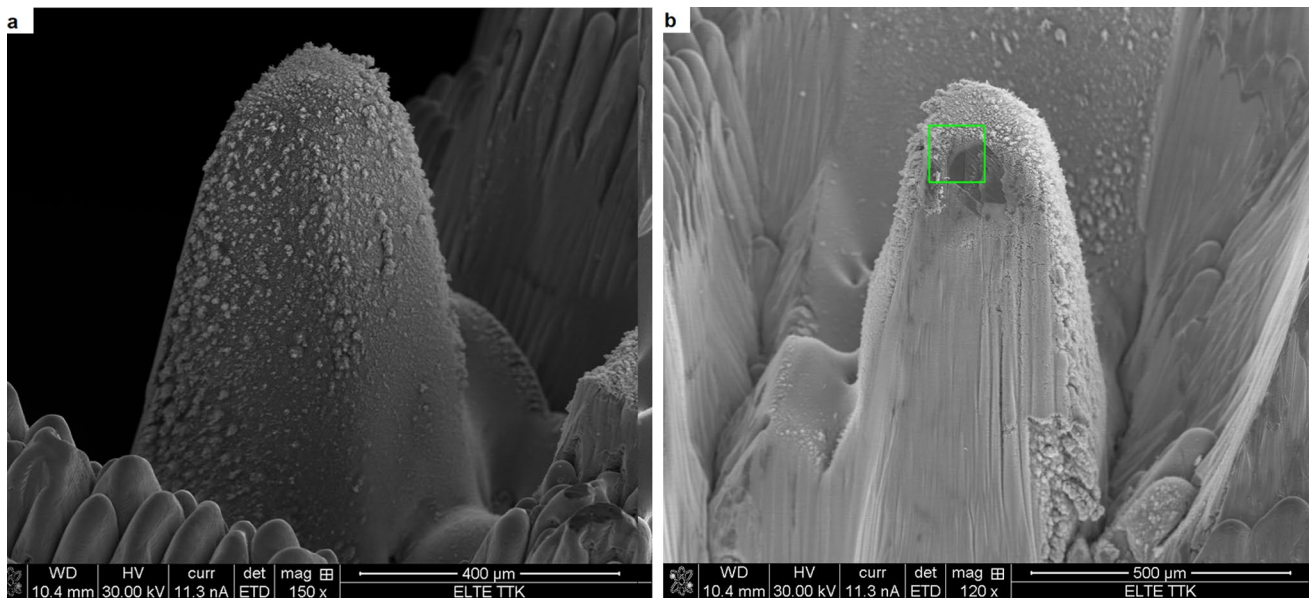


Fig. 5 Top: a pillar fabricated by laser ablation. Bottom: a small part of the top of the pillar was slightly FIB polished for EBSD measurement. Its vicinity is indicated by the green rectangle

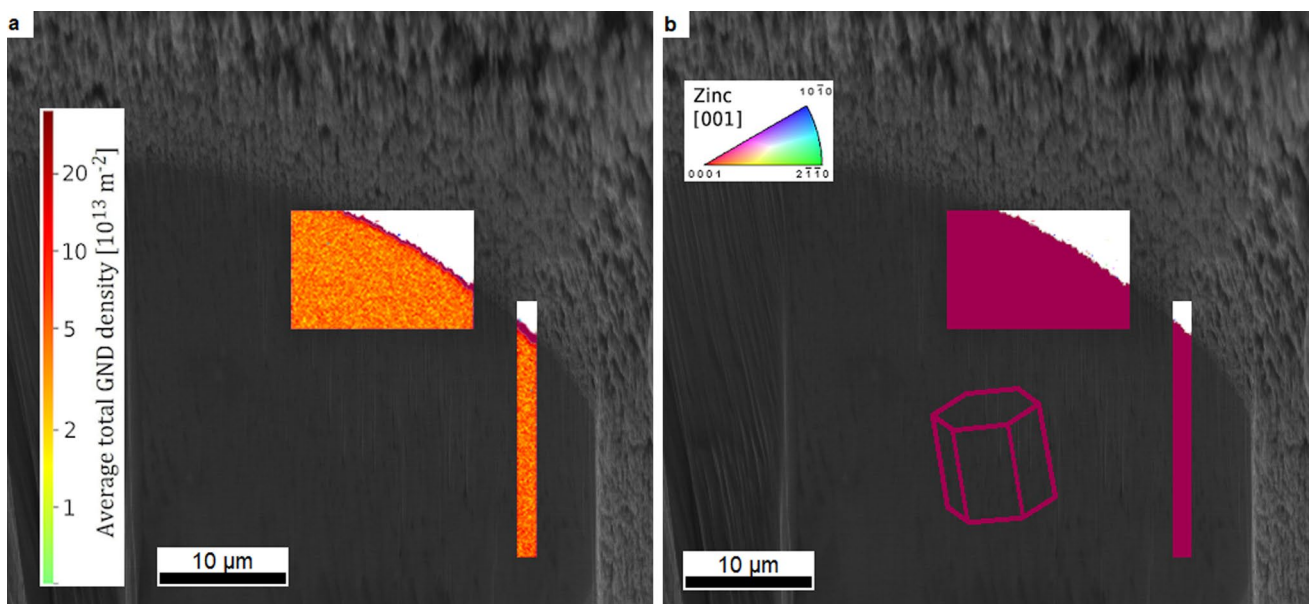


Fig. 6 EBSD measurement of a pillar. The applied resolution (step size of the EBSD mapping) was 120 nm. Top: the measured GND density is found to be constant in space. Bottom: orientation map shows that the crystal orientation is homogeneous

micromachining processes. For instance, compared to [35], we used a laser beam that was normal to the sample surface, and we used a flat-top beam profile laser system. In our case the energy density, that determines the ablation rate, and according to [60] determines crystal damage as well, was constant in space due to the flat-top beam profile. The total energy per pulse, which can be another parameter

of fundamental importance, was at least a magnitude higher than used by others for pillar fabrication [23–29].

We compared our experimental results about the thickness of the HAZ with results of temperature simulations described in section 3. In the simulations the region where the temperature got elevated significantly is considered to be the HAZ. Using an energy density value of 10 J/cm², the

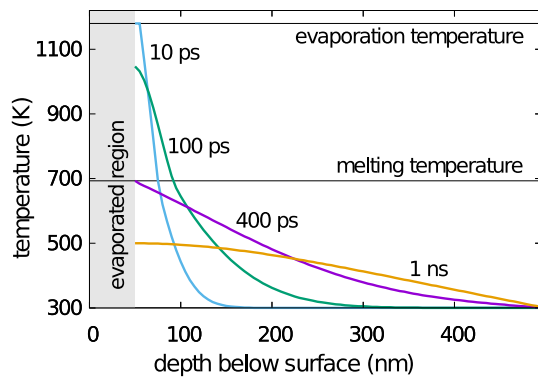


Fig. 7 Computer simulated temperature distributions as a function of the depth. The curves correspond to different times after the laser pulse. The upper layer that's temperature exceeds the evaporation temperature is considered to be removed. Only temperature values below the evaporation temperature are plotted

results obtained are shown in Fig. 7. We consider the HAZ to be the region where the temperature got elevated significantly (100–200 K). Thus simulated thickness of the HAZ is only a few hundreds of nanometers, which corresponds to the results of our experiments.

It is important to note that the surface of the pillar, particularly its top, is covered by redeposited material. While creating the FIB-polished surface it was found that the material removal rate of FIB milling was two times lower in the case of the redeposited shell, which was several micrometers thick. To remove easily this outer shell and to create an object with a crystalline surface an electropolishing process was applied, too. The conditions of this polishing method were similar to the parameters used for the preparation of the single crystal, mentioned above. The only difference was that the applied duration was reduced to 5 s. This electropolishing resulted in the removal of all the redeposited porous layer, but it was short enough to preserve the original shape of the laser-formed pillar, see Fig. 8.

5 Conclusion

Surface micromachining was performed using a laser system with femtosecond pulses. Columns (micropillars) were ablated into the surface of zinc samples. For this, a hybrid dye-excimer laser system, that has high output energy (tens of mJ) with a flat-top beam profile, and relatively low repetition rate (maximum 2 Hz), was used. Material microstructure degradation was studied using SEM and HR-EBSD techniques.

Two methods were tested for micromachining. First a mask was projected onto the surface of a standing sample. It was shown that the production of free-standing objects,

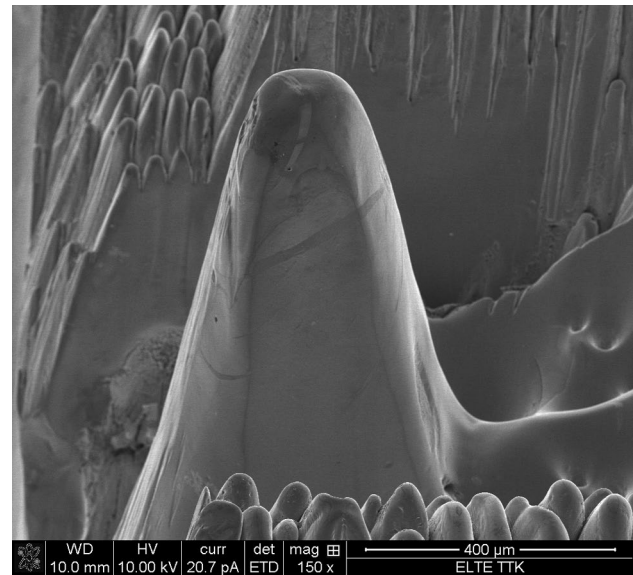


Fig. 8 SEM image of a pillar with the redeposited layer removed using electropolishing

like micropillars for compression tests, is not possible this way: after the ablation with multiple pulses a large, conical structure remains around the fabricated object.

In the second method, the beam was scanned several times around the prospective pillar, creating a ditch around the unablated area. This method resulted in a rather flat ditch without the appearance of a structure consisting of cones, and free-standing pillars were fabricated. It means that the conical structure that is commonly observed after femtosecond laser ablation of the very same spot are mainly the consequence of beam inhomogeneities of our system, thus can be avoided by scanning the laser beam.

The damage of the crystalline microstructure of the fabricated pillar was examined by a HR-EBSD measurement. It was found that below the redeposition a thin layer is observable. This layer was associated with the heat affected zone. The underlying material was unaltered during the laser ablation. This result represents the capability of this laser ablation process to maintain not only single crystal structure but other characteristics like dislocation density as well. Further investigations revealed that the laser generated, few μm thick porous, redeposited layer could easily be removed by a slight, rapid electropolishing that yields no significant changes in the sample's shape.

This way of laser ablation with this high energy (20 mJ) per pulse, UV, ultrashort pulsed laser system is an appropriate and feasible tool to fabricate or prefabricate surface structures that have undamaged single crystal structure. To create an object with an exact shape, like a straight pillar, further, lower scale machining might be necessary. In case of pillars for compression tests, this further FIB machining

is significantly simpler and faster than FIB only fabrication of pillars. Hence the shape of the pillar has been created by laser ablation, and FIB milling of a vertical wall is faster than trenching. Furthermore most part of the material has already been removed by laser ablation.

Acknowledgements Project no. TKP2021-NVA-16 has been implemented with the support provided by the Ministry of Innovation and Technology of Hungary from the National Research, Development and Innovation Fund. This work was supported by the National Research, Development and Innovation Office (OTKA K138339 project) of Hungary.

Author contributions All authors contributed to the study conception and design. Material preparation was performed by DU, PIS, BG and ZH performed the laser ablation experiments. DU, ZD, SL and ZT performed the microscopy with PIS. The manuscript was mainly written by PIS and ZT and all authors commented on it. All authors read and approved the final manuscript.

Funding Open access funding provided by National University of Public Service.

Data Availability Data sets generated during the current study are available from the corresponding author on reasonable request.

Declarations

Conflict of interest The authors have no conflicts of interest to declare that are relevant to the content of this article.

Open Access This article is licensed under a Creative Commons Attribution 4.0 International License, which permits use, sharing, adaptation, distribution and reproduction in any medium or format, as long as you give appropriate credit to the original author(s) and the source, provide a link to the Creative Commons licence, and indicate if changes were made. The images or other third party material in this article are included in the article's Creative Commons licence, unless indicated otherwise in a credit line to the material. If material is not included in the article's Creative Commons licence and your intended use is not permitted by statutory regulation or exceeds the permitted use, you will need to obtain permission directly from the copyright holder. To view a copy of this licence, visit <http://creativecommons.org/licenses/by/4.0/>.

References

1. B.N. Chichkov, C. Momma, S. Nolte, F. Von Alvensleben, A. Tunnermann, Femtosecond, picosecond and nanosecond laser ablation of solids. *Appl. Phys. A* **63**(2), 109–115 (1996)
2. D. Bäuerle, *Laser Processing and Chemistry* (Springer, New York, 2013)
3. B. Borchers, J. Bekesi, P. Simon, J. Ihlemann, Submicron surface patterning by laser ablation with short uv pulses using a proximity phase mask setup. *J. Appl. Phys.* **107**(6), 063106 (2010)
4. D.M. Dimiduk, C. Woodward, R. LeSar, M.D. Uchic, Scale-free intermittent flow in crystal plasticity. *Science* **312**(5777), 1188–1190 (2006)
5. F.F. Csikor, C. Motz, D. Weygand, M. Zaiser, S. Zapperi, Dislocation avalanches, strain bursts, and the problem of plastic forming at the micrometer scale. *Science* **318**(5848), 251–254 (2007)
6. M.D. Uchic, D.M. Dimiduk, N.F. Jeffrey, D.N. William, Sample dimensions influence strength and crystal plasticity. *Science* **305**(5686), 986–989 (2004)
7. J. Ye, J. Lu, C. Liu, Q. Wang, Y. Yang, Atomistic free-volume zones and inelastic deformation of metallic glasses. *Nat. Mater.* **9**(8), 619–623 (2010)
8. P.J. Imrich, C. Kirchlechner, C. Motz, G. Dehm, Differences in deformation behavior of bicrystalline cu micropillars containing a twin boundary or a large-angle grain boundary. *Acta Mater.* **73**, 240–250 (2014)
9. K. Máthi, M. Knapek, F. Šiška, P. Hrcubca, D. Ugi, P.D. Ispánovity, I. Groma, K.S. Shin, On the dynamics of twinning in magnesium micropillars. *Mater Design* **203**, 109563 (2021)
10. D. Kiener, W. Grosinger, G. Dehm, R. Pippan, A further step towards an understanding of size-dependent crystal plasticity: In situ tension experiments of miniaturized single-crystal copper samples. *Acta Mater.* **56**(3), 580–592 (2008)
11. T. Ajantiwalay, H. Vo, R. Finkelstein, P. Hosemann, A. Aitkaliyeva, Towards bridging the experimental length-scale gap for tensile tests on structural materials: Lessons learned from an initial assessment of microtensile tests and the path forward. *JOM* **72**(1), 113–122 (2020)
12. B. Bellón, S. Haouala, J. LLorca, An analysis of the influence of the precipitate type on the mechanical behavior of al-cu alloys by means of micropillar compression tests. *Acta Materialia* **194**, 207–223 (2020)
13. H. Jones, V. Tong, R. Ramachandramoorthy, K. Mingard, J. Michler, M. Gee, Micropillar compression of single crystal tungsten carbide, part 1: Temperature and orientation dependence of deformation behaviour. *Int. J. Refract Metal Hard Mater.* **102**, 105729 (2022)
14. D. Kiener, C. Motz, G. Dehm, Micro-compression testing: A critical discussion of experimental constraints. *Mater. Sci. Eng., A* **505**(1), 79–87 (2009)
15. P.D. Ispánovity, I. Groma, G. Györgyi, P. Szabó, W. Hoffelner, Criticality of relaxation in dislocation systems. *Phys. Rev. Lett.* **107**(8), 085506 (2011)
16. M.D. Uchic, P.A. Shade, D.M. Dimiduk, Plasticity of micrometer-scale single crystals in compression. *Annu. Rev. Mater. Res.* **39**(1), 361–386 (2009)
17. X. Ma, Q. Jiao, L.J. Kecskes, J.A. El-Awady, T.P. Weihs, Effect of basal precipitates on extension twinning and pyramidal slip: A micro-mechanical and electron microscopy study of a mg-al binary alloy. *Acta Mater.* **189**, 35–46 (2020)
18. R. Maaß, M. Wraith, J. Uhl, J. Greer, K. Dahmen, Slip statistics of dislocation avalanches under different loading modes. *Phys. Rev. E* **91**(4), 042403 (2015)
19. M. Chelu, H. Stroescu, M. Anastasescu, J.M. Calderon-Moreno, S. Preda, M. Stoica, Z. Fogarassy, P. Petrik, M. Gheorghe, C. Parvulescu, C. Brasoveanu, A. Dinescu, C. Moldovan, M. Gartner, High-quality pmma/zno nws piezoelectric coating on rigid and flexible metallic substrates. *Appl. Surf. Sci.* **529**, 147135 (2020)
20. L. Pastewka, R. Salzer, A. Graff, F. Altmann, M. Moseler, Surface amorphization, sputter rate, and intrinsic stresses of silicon during low energy ga+ focused-ion beam milling. *Nucl. Instrum. Methods Phys. Res., Sect. B* **267**(18), 3072–3075 (2009)
21. S. Shim, H. Bei, M.K. Miller, G.M. Pharr, E.P. George, Effects of focused ion beam milling on the compressive behavior of directionally solidified micropillars and the nanoindentation response of an electropolished surface. *Acta Mater.* **57**(2), 503–510 (2009)
22. T. Ishitani, K. Umemura, T. Ohnishi, T. Yaguchi, T. Kamino, Improvements in performance of focused ion beam cross-sectioning: aspects of ion-sample interaction. *Microscopy* **53**(5), 443–449 (2004)

23. Q. McCulloch, J. Gigax, P. Hosemann, Femtosecond laser ablation for mesoscale specimen evaluation. *JOM* **72**(4), 1694–1702 (2020)
24. Z. Lin, D. Magagnosc, J. Wen, C.-S. Oh, S.-M. Kim, H. Espinosa, In-situ sem high strain rate testing of large diameter micropillars followed by tem and ebsd postmortem analysis. *Exper Mech.* **61**, 1–14 (2021)
25. J.G. Gigax, H. Vo, Q. McCulloch, M. Chancey, Y. Wang, S.A. Maloy, N. Li, P. Hosemann, Micropillar compression response of femtosecond laser-cut single crystal cu and proton irradiated cu. *Scripta Mater.* **170**, 145–149 (2019)
26. R. Barnett, S. Mueller, S. Hiller, F. Perez-Willard, J. Strickland, H. Dong, Rapid production of pillar structures on the surface of single crystal cmsx-4 superalloy by femtosecond laser machining. *Opt. Lasers Eng.* **127**, 105941 (2020)
27. S. Jakob, M.J. Pfeifenberger, A. Hohenwarter, R. Pippan, Femtosecond laser machining for characterization of local mechanical properties of biomaterials: a case study on wood. *Sci. Technol. Adv. Mater.* **18**(1), 574–583 (2017)
28. B. Tordoff, C. Hartfield, A.J. Holwell, S. Hiller, M. Kaestner, S. Kelly, J. Lee, S. Müller, F. Perez-Willard, T. Volkenandt, The laserfib: new application opportunities combining a high-performance fib-sem with femtosecond laser processing in an integrated second chamber. *Appl. Microscopy* **50**(1), 1–11 (2020)
29. J.G. Gigax, A.J. Torrez, Q. McCulloch, H. Kim, S.A. Maloy, N. Li, Sizing up mechanical testing: Comparison of microscale and mesoscale mechanical testing techniques on a fecral welded tube. *J. Mater. Res.* **35**(20), 2817–2830 (2020)
30. A. Dong, J. Duckering, J. Peterson, S. Lam, D. Routledge, P. Hosemann, Femtosecond laser machining of micromechanical tensile test specimens. *JOM* **73**(12), 4231–4239 (2021)
31. M.J. Pfeifenberger, M. Mangang, S. Wurster, J. Reiser, A. Hohenwarter, W. Pflöging, D. Kiener, R. Pippan, The use of femtosecond laser ablation as a novel tool for rapid micro-mechanical sample preparation. *Mater. Design* **121**, 109–118 (2017)
32. S.N. Bhavsar, S. Aravindan, P.V. Rao, Investigating material removal rate and surface roughness using multi-objective optimization for focused ion beam (fib) micro-milling of cemented carbide. *Precis. Eng.* **40**, 131–138 (2015)
33. Y. Hirayama, M. Obara, Heat-affected zone and ablation rate of copper ablated with femtosecond laser. *J. Appl. Phys.* **97**(6), 064903 (2005)
34. M.S. Titus, M.P. Echlin, P. Gumbsch, T.M. Pollock, Dislocation injection in strontium titanate by femtosecond laser pulses. *J. Appl. Phys.* **118**(7), 075901 (2015)
35. M.P. Echlin, M.S. Titus, M. Straw, P. Gumbsch, T.M. Pollock, Materials response to glancing incidence femtosecond laser ablation. *Acta Mater.* **124**, 37–46 (2017)
36. S. Szatmari, F. Schäfer, Simplified laser system for the generation of 60 fs pulses at 248 nm. *Optics Commun.* **68**(3), 196–202 (1988)
37. S. Szatmari, High-brightness ultraviolet excimer lasers. *Appl. Phys. B* **58**(3), 211–223 (1994)
38. P.D. Ispánovity, D. Ugi, G. Péterffy, M. Knapek, S. Kalácska, D. Tüzes, Z. Dankházi, K. Máthi, F. Chmelík, I. Groma, Dislocation avalanches are like earthquakes on the micron scale. *Nat. Commun.* **13**(1), 1–10 (2022)
39. J. Byskov-Nielsen, J.-M. Savolainen, M.S. Christensen, P. Balling, Ultra-short pulse laser ablation of copper, silver and tungsten: experimental data and two-temperature model simulations. *Appl. Phys. A* **103**(2), 447–453 (2011)
40. J. Budai, Z. Pápa, P. Petrik, P. Dombi, Ultrasensitive probing of plasmonic hot electron occupancies. *Nat. Commun.* **13**(1), 6695 (2022)
41. C. Wu, L.V. Zhigilei, Microscopic mechanisms of laser spallation and ablation of metal targets from large-scale molecular dynamics simulations. *Appl. Phys. A* **114**(1), 11–32 (2014)
42. A.K. Jain, V. Kulkarni, D. Sood, Pulsed laser heating calculations incorporating vapourization. *Appl. Phys.* **25**(2), 127–133 (1981)
43. Z. Toth, T. Szörényi, Pulsed laser processing of ge/se thin film structures. *Appl. Phys. A* **52**(4), 273–279 (1991)
44. Á.I. Hegyi, P.D. Ispánovity, M. Knapek, D. Tüzes, K. Máthi, F. Chmelík, Z. Dankházi, G. Varga, I. Groma, Micron-scale deformation: A coupled in situ study of strain bursts and acoustic emission. *Microsc. Microanal.* **23**(6), 1076–1081 (2017)
45. S. Preuss, A. Demchuk, M. Stuke, Sub-picosecond uv laser ablation of metals. *Appl. Phys. A* **61**(1), 33–37 (1995)
46. M. Hashida, A. Semerok, O. Gobert, G. Petite, Y. Izawa, Ablation threshold dependence on pulse duration for copper. *Appl. Surf. Sci.* **197**, 862–867 (2002)
47. N. Nedialkov, P. Atanasov, S. Amoruso, R. Bruzzese, X. Wang, Laser ablation of metals by femtosecond pulses: Theoretical and experimental study. *Appl. Surf. Sci.* **253**(19), 7761–7766 (2007)
48. J. Byskov-Nielsen, J.-M. Savolainen, M.S. Christensen, P. Balling, Ultra-short pulse laser ablation of metals: threshold fluence, incubation coefficient and ablation rates. *Appl. Phys. A* **101**(1), 97–101 (2010)
49. S. Tani, Y. Kobayashi, Pulse-by-pulse depth profile measurement of femtosecond laser ablation on copper. *Appl. Phys. A* **124**(3), 1–5 (2018)
50. L. Museur, A. Manousaki, D. Anglos, T. Chauveau, A. Kanaev, Effect of laser polarization and crystalline orientation on zno surface nanostructuring in the regime of high-density electronic excitation. *JOSA B* **31**(11), 44–47 (2014)
51. K. Ahmmed, C. Grambow, A.-M. Kietzig, Fabrication of micro/nano structures on metals by femtosecond laser micromachining. *Micromachines* **5**(4), 1219–1253 (2014)
52. B.K. Nayak, M.C. Gupta, Self-organized micro/nano structures in metal surfaces by ultrafast laser irradiation. *Opt. Lasers Eng.* **48**(10), 940–949 (2010)
53. C.A. Zuhlke, T.P. Anderson, D.R. Alexander, Fundamentals of layered nanoparticle covered pyramidal structures formed on nickel during femtosecond laser surface interactions. *Appl. Surf. Sci.* **283**, 648–653 (2013)
54. N. Semmar, A. Talbi, M. Mikikian, A. Stolz, A. Melhem, D. de Sousa Meneses, Micro-spikes formed on mesoporous silicon by uv picosecond laser irradiation. *Appl. Surf. Sci.* **509**, 144820 (2020)
55. P. Simon, J.H. Klein-Wiele, Vorrichtung und Verfahren zur Strahlhomogenisierung von Ultrakurzpulslasern (DE10249532, Deutsches Patent- und Markenamt (2004))
56. T. Britton, A.J. Wilkinson, High resolution electron backscatter diffraction measurements of elastic strain variations in the presence of larger lattice rotations. *Ultramicroscopy* **114**, 82–95 (2012)
57. J.F. Nye, Some geometrical relations in dislocated crystals. *Acta Metall.* **1**(2), 153–162 (1953)
58. A.J. Wilkinson, D. Randman, Determination of elastic strain fields and geometrically necessary dislocation distributions near nanoindenters using electron back scatter diffraction. *Phil. Mag.* **90**(9), 1159–1177 (2010)
59. D. Wallis, L.N. Hansen, A.J. Wilkinson, R.A. Lebensohn, Dislocation interactions in olivine control postseismic creep of the upper mantle. *Nat. Commun.* **12**(1), 1–12 (2021)
60. T. Matsuda, T. Sano, K. Arakawa, O. Sakata, H. Tajiri, A. Hirose, Femtosecond laser-driven shock-induced dislocation structures in iron. *Appl. Phys. Express* **7**(12), 122704 (2014)